energies

MDPI

*Article*

# Simulation, Analysis, and Characterization of Calcium-Doped ZnO Nanostructures for Dye-Sensitized Solar Cells

**Shahzadi Tayyaba [1], Muhammad Waseem Ashraf [2,*], Muhammad Imran Tariq [3], Maham Akhlaq [2], Valentina Emilia Balas [4,*], Ning Wang [5] and Marius M. Balas [4]**

1 Department of Computer Engineering, The University of Lahore, Lahore 54000, Pakistan; Shahzadi.Tayyaba@hotmail.com
2 Department of Physics (Electronics), GC University Lahore, Lahore 54000, Pakistan; maham_9458@hotmail.com
3 Department of Computer Science, The Superior University Lahore, Lahore 54000, Pakistan; imrantariqbutt@yahoo.com
4 Automatics and Applied Software Department, "Aurel Vlaicu" University of Arad, 310130 Arad, Romania; marius.balas@uav.ro
5 Center for Green Innovation, School of Mathematics and Physics, University of Science and Technology Beijing, Beijing 100069, China; wangning@ustb.edu.cn
* Correspondence: muhamamd.waseem.ashraf@gmail.com (M.W.A.); balas@drbalas.ro (V.E.B.)

Received: 8 May 2020; Accepted: 11 September 2020; Published: 17 September 2020


**Abstract:** In this research article, the authors have discussed the simulation, analysis, and characterization of calcium-doped zinc oxide (Ca-doped-ZnO) nanostructures for advanced generation solar cells. A comparative study has been performed to envisage the effect of Ca-doped ZnO nanoparticles (NP), seeded Ca-doped ZnO nanorods (NR), and unseeded Ca-doped ZnO NR as photoanodes in dye-sensitized solar cells. Simulations were performed in MATLAB fuzzy logic controller to study the effect of various structures on the overall solar cell efficiency. The simulation results show an error of less than 1% in between the simulated and calculated values. This work shows that the diameter of the seeded Ca-doped ZnO NR is greater than that of the unseeded Ca-doped ZnO NR. The incorporation of Ca in the ZnO nanostructure is confirmed using XRD graphs and an EDX spectrum. The optical band gap of the seeded substrate is 3.18 eV, which is higher compared to those of unseeded Ca-doped ZnO NR and Ca-doped ZnO NP, which are 3.16 eV and 3.13 ev, respectively. The increase in optical band gap results in the improvement of the overall solar cell efficiency of the seeded Ca-doped ZnO NR to 1.55%. The incorporation of a seed layer with Ca-doped ZnO NR increases the fill factor and the overall efficiency of dye-sensitized solar cells (DSSC).

**Keywords:** DSSC; chemical bath deposition; Ca-doped ZnO; nanorods

## 1. Introduction

Due to prevailing energy requirements, the necessity of a clean energy technology is substantial. The use of photovoltaic (PV) solar cells is considered as one of the most suitable ways for the generation of clean energy technology [1]. Mostly, PV solar cells are found in three major types including high-efficiency silicon solar cell, thin film solar cell, and advanced generation solar cell. Among advanced generation solar cells, dye-sensitized solar cells (DSSC) are an emerging type of advanced generation solar cells. They are considered as an alternate to silicon solar cells due to their easy and low-cost fabrication [2]. DSSC comprises of a mesoporous dye-loaded photoanode, electrolyte, and a counter electrode. The photogeneration of an electron hole pair is carried out by the

dye. The dye molecules attached to the mesoporous photoanode absorb the photon to create an excited electronic state. Furthermore, the injection of the electrons takes place from the dye molecule to the conduction band of the semi-conductor photoanode, keeping the dye in its oxidizing state, as shown in Figure 1. At electrolyte, the redox reaction takes place that reduces the dye back to its neutral state [3]. The semi-conductor photoanode transfers the electron to the counter electrode or cathode via the external circuit [4]. The cathode moves the electron to the electrolyte. At the electrode, the reduction reaction takes place, and electrolyte restores to its neutral state by accepting electrons from the external circuit [5].

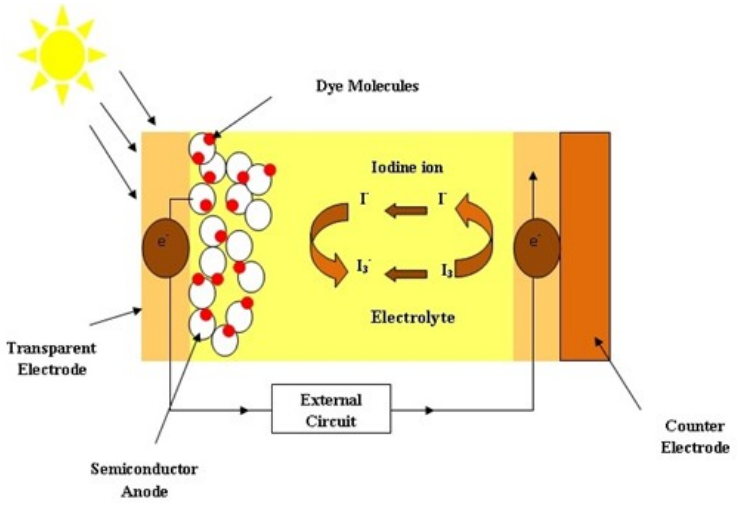


**Figure 1.** Working of a typical dye-sensitized solar cell.

Initially, bulk semi-conductor materials were used as photoanode. However, these materials show photocorrosion when exposed to sunlight, which highly affects the stability of the cell. To diminish these concerns, wide band-gap nanostructured semi-conductors/metal oxides are used. These newly employed structures show resistance toward photocorrosion. Furthermore, these materials manifest spectacular optical and electrical properties. Multiple metal oxide-based nanostructures including nanoparticles, nanospheres, nanorods, and nanofibers are used for the semi-conductor anode in DSSC. Metal oxides mainly comprise titanium dioxide ($TiO_2$) [6–8], tin oxide ($SnO_2$) [9], zinc oxide (ZnO) [10,11], Niobium pentaoxide ($Nb_2O_3$) [12], and composite-based metal oxides. Among various metal oxide nanostructures, nanoparticles provide a better surface area to volume ratio. However, due to grain boundaries, the hindering of electron transfer happens in nanoparticles. In this case, nanorods-based structures provide continuous charge transfer, which makes them suitable for DSSC [13].

Among various metal oxide materials, ZnO is considered as an advanced and efficient material due to its wider band gap, low cost, and easy fabrication. ZnO shows excellent piezo and pyro electric properties. It has vast applications as an energy harvester, solar cell, in electronic devices, and in the biomedical field [14–16]. ZnO is considered as an excellent material that can be converted into various nanostructures including nanoparticles, nanorods, nanowires, nanotubes, and nanoflowers with a large surface area to volume ratio [17,18]. Nanoparticles-based structures provide a large surface area to volume ratio; however, due to grain defects, these types of nanostructures do not provide efficient output. Among other nanostructures, ZnO nanorods-based structures are considered as an efficient structure that can be deployed in advanced generation solar cells mainly due to continuous charge transfer. These nanorods can be fabricated using various methods including hydrothermal synthesis [19], electrochemical synthesis [20], chemical vapor deposition [21], pulsed laser ablation, physical vapor deposition [22], and chemical bath deposition [23]. Among these methods, chemical bath deposition is considered as an efficient and easy method for the smooth thin film fabrication of nanorods. The process parameters can easily be controlled using the chemical bath deposition

process, which make it an excellent method for the fabrication of nanorods. The doping of ZnO with a second group including magnesium, calcium, beryllium, and strontium elements has been considered as an effective technique to varying the structural, optical, and electrical properties of ZnO [24–26]. Majeed Gul [27] et al. reported the band-gap tuning of ZnO nanorods by the addition of Mg from 3.18 eV to 3.32 eV. Similarly, with strontium doping, the band gap can be reduced, and the solar cell efficiency of the DSSC can be enhanced. Similarly, calcium and beryllium can be used to enhance the particle size and optical properties of ZnO nanostructures. Various simulation tools are used for the parametric estimation and power conversion efficiency comparison of the prepared nanostructures including ANSYS, COMSOL, ABAQUS, and MATLAB fuzzy logic controller [28–30]. Among other methods, fuzzy logic controller is considered as an efficient and easy technique that is close to human thinking. It is considered as an efficient method to interpret the output values based on real-life conditions.

In this work, a comparative study has been performed to study the overall solar cell efficiency of Ca-doped ZnO nanoparticles deposited using spin-coating and Ca-doped ZnO nanorods fabricated using chemical bath deposition. The parametric estimation is conducted on the basis of the fuzzy logic tool. The effect of the seed layer of ZnO has also been studied to see its effect on the total solar cell efficiency.

## 2. Fuzzy Analysis

Fuzzy analysis of the Ca-doped ZnO nanoparticles (NP) and seeded and unseeded Ca-doped ZnO nanorods (NR)-based photoanodes have been performed using the MAMDAMI model. The fuzzy inference system (FIS) diagrams of the three samples are shown in Figure 2. Figure 2a shows the input of the first fuzzy analysis. The Ca-doped ZnO NP size and annealing temperature are taken as input. The effects of the two inputs are studied on the band gap and power conversion efficiency of the solar cell. Similarly, the effect of the diameter of the Ca-doped ZnO NR and annealing temperature are studied on the band gap and power conversion efficiency for seeded and unseeded substrates.

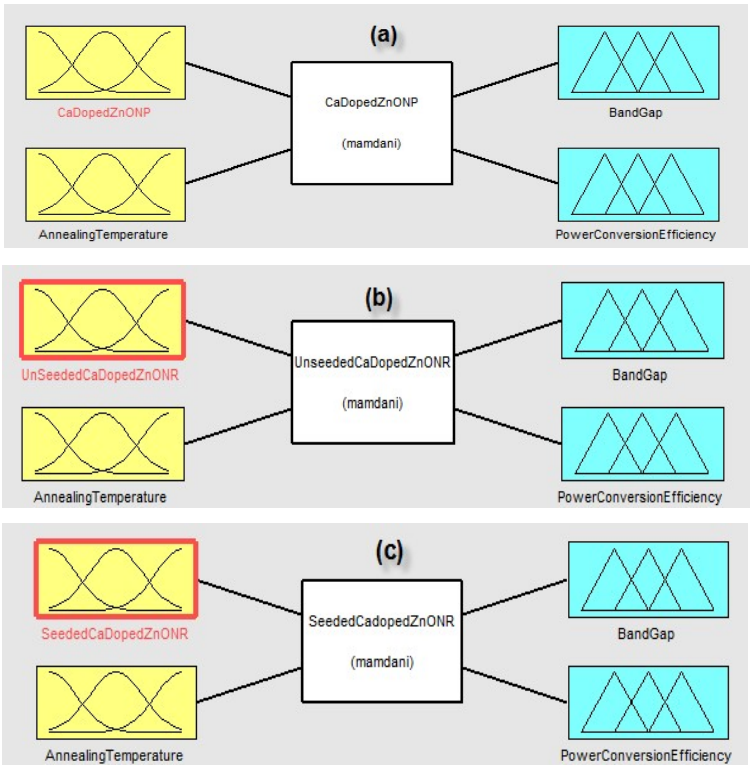


**Figure 2.** FIS figure for (**a**) Ca-doped ZnO nanoparticles (NP) and (**b**) Unseeded Ca-doped ZnO nanorods (NR) (**c**) Seeded Ca-doped ZnO NR.

The ranges and membership functions are assigned to the respective inputs and outputs. The range for the input annealing temperature in all the three models is 400–500 °C. For Ca-doped ZnO nanoparticles, the range is 120–140 nm. For unseeded Ca-doped ZnO nanorods and seeded Ca-doped ZnO nanorods, the range for the input is 100–200 nm. The range for band gap was 3.1 to 3.2 eV, and for power conversion efficiency, the range is 1% to 2%. Then, rules for the memberships functions are added to the fuzzy simulations. The numbers of rules is based on the number of input. Figure 3 shows the 3D graphs for the respective Ca-doped ZnO nanostructure-based photoanodes. Figure 3a,b shows the effect of Ca-doped ZnO nanoparticles and annealing temperature on band gap and power conversion efficiency. Figure 3c,d shows the effect of unseeded Ca-doped ZnO nanorods and annealing temperature on band gap and power conversion efficiency. Figure 3e,f shows the effect of seeded Ca-doped ZnO nanorods and annealing temperature on band gap and power conversion efficiency. The increase in particle size and the nanorods diameter directly decreases the band gap. The effect predominantly appears due to the quantum confinement effect.

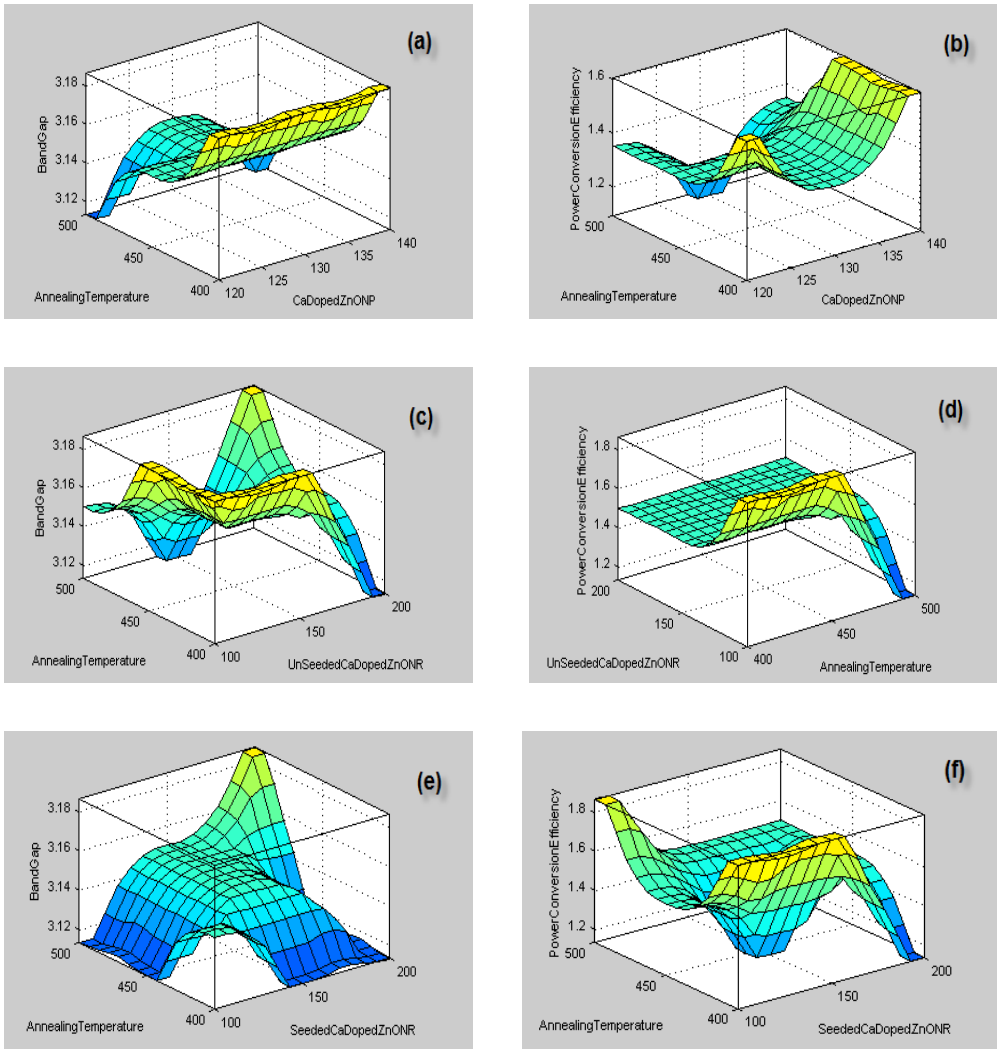


**Figure 3.** 3D graphs of band gap and power conversion efficiency and its effect on (**a**,**b**) Annealing temperature and Ca-doped ZnO NP; (**c**,**d**) Annealing temperature and unseeded Ca-doped ZnO NR; (**e**,**f**) Annealing temperature and seeded Ca-doped ZnO NR.

The simulation results are shown using the rule viewer. The annealing temperature is set at 500 °C as used in the experiment. Figure 4 shows the crisp input values and the corresponding output values based on the rules.

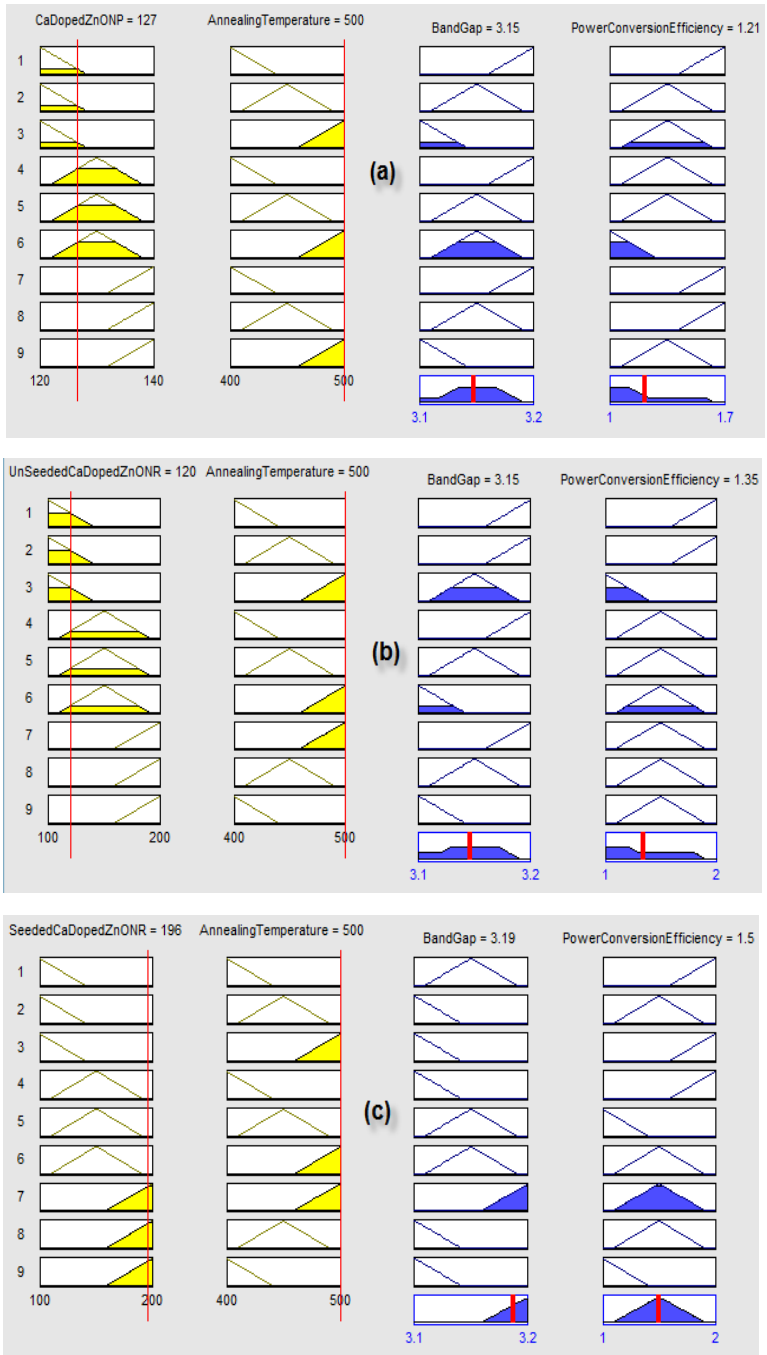


**Figure 4.** Rule Viewer: (**a**) Ca-doped ZnO NP; (**b**) Unseeded Ca-doped ZnO NR; (**c**) Seeded Ca-doped ZnO NR.

The simulation results from the rule viewer are compared with the theoretical values using the MAMDANI model formula,

$$\text{MAMDANI Model} = [\ \Sigma\ (\text{Mi} \times \text{Si})/\text{Mi}] \times 100$$

where Mi is the membership function value and Si is the singleton value. Table 1 shows the comparison and error between the simulated and calculated theoretical value.

**Table 1.** Comparison between simulated and calculated values.

| | Simulated Value | | Calculated Value | | Error | |
|---|---|---|---|---|---|---|
| | **Band Gap (eV)** | **PCE (%)** | **Band Gap (eV)** | **PCE (%)** | **Band Gap (eV)** | **PCE (%)** |
| Ca-doped ZnO NP | 3.15 | 1.21 | 3.13 | 1.22 | 0.7 | 0.9 |
| Unseeded Ca-doped ZnO NR | 3.15 | 1.34 | 3.15 | 1.35 | 0 | 0.8 |
| Seeded Ca-doped ZnO NR | 3.19 | 1.5 | 3.2 | 1.51 | 0.4 | 0.7 |

The table shows the accuracy of the simulated and calculated value with an error less than 1% between the values.

## 3. Materials and Methods

Zinc acetate di-hydrate, methoxyethanol, hexamethylenetetramine, and calcium acetate have been used to carry out the experimental work. Indium tin oxide glass was used as a substrate. N3 Ruthenium has been used as a dye for DSSC fabrication. 2-Propanol and deionized (DI) water were used as solvent for the synthesis of photoanode. The spin-coating method was used to fabricate the ZnO nanoparticles layer, while ZnO nanorods were fabricated using the chemical bath deposition method [31,32].

*Photoanode Preparation*

The 2 cm × 2 cm ITO glass was pre-cleaned using DI water, acetone, and ethanol. The glass was initially cleaned with soap and furthermore sonicated in ethanol, DI water, and acetone for 20 min. For ZnO nanoparticle-based photoanodes, 20 mM solution of zinc acetate dehydrate was prepared in 2-propanol with 2% doping of Ca. The solution was stirred at 45 °C for 2 h. Then, 2–3 drops of methoxyethanol were added to get a transparent solution. The prepared solution was aged for 24 h before being spin-coated on the ITO glass. The solution was added dropwise on the substrate, which was furthermore spun at a rate of 2500 rpm for 20 s Then, the substrate was heated at 90 °C for the complete evaporation of the solvent. The process was repeated 10 times to get a clear thin film of ZnO nanoparticles. Then, the substrate was subjected to annealing at 500 °C for 2 h to get a thin film of ZnO nanoparticles.

For the preparation of ZnO nanorods, 2 substrates were fabricated. One of the substrates is directly subjected to the growth of ZnO nanorods, and the other substrate is first seeded. For seeding, the substrate is subjected to the above stated spin-coating process without the addition of Ca doping. For nanorods growth, 20 mM zinc acetate di-hydrate and hexamethylenetetramine solution was made in DI water with 2% calcium doping. The solution was added to the double-wall beaker of the chemical bath deposition (CBD) setup. The seeded and unseeded substrate was inserted in the beaker using a Teflon holder. The CBD temperature was set at 90 °C with continuous stirring at 400 rpm for 4 h. Then, the substrate was washed with DI water and annealed at 500 °C with a 5 °C rise per minute. The Ca-doped ZnO nanoparticles and nanorods-based samples prepared are shown in Table 2.

**Table 2.** Samples prepared for Ca-doped ZnO NP and NR.

| Sample Name | ZnO Seeding Layer | Ca-Doped ZnO NP | Ca-Doped ZnO NR |
|---|---|---|---|
| $Z_1$ | X | √ | X |
| $Z_2$ | X | X | √ |
| $Z_3$ | √ | X | √ |

For device fabrication, the prepared photoanodes of Ca-doped ZnO NP, seeded NR, and unseeded NR are dipped in dye solution. The anodes are dipped for 2 h in N3 ruthenium dye solution for better absorption of dye molecules. Gold is used as a counter electrode, while the substrate was ITO-coated. The anode and electrode are clipped together, and redox electrolyte is inserted. Three sets of each samples are produced, and the results are calculated on the basis of the average of the results.

The prepared photoanodes are characterized using scanning electron microscopy (SEM) and energy dispersive X-ray spectroscopy (EDX) to study their morphology and chemical composition. Similarly, UV-Vis spectrophotometry is used to analyze the optical properties of the prepared photoanode. For IV measurements including open circuit voltage and short circuit current, a solar simulator is used with light intensity similar to sunlight. The DSSCs photovoltaic parameters including open-circuit voltage (Voc), the short-circuit current density (Jsc), the fill factor (FF), and the photoconversion efficiency were studied through the I-V measurements. The I-V measurements were conducted using a source measure unit (Keithley 2400) and a solar simulator (Keithlink) under a power intensity of 750 W/m$^2$.

## 4. Results and Discussion

The scanning electron microscopy of the Ca-doped ZnO nanoparticles is shown in Figure 5. The figure confirms the formation of nanoparticles, which are agglomerated together to form a large cluster. The average nanoparticles size was estimated during SEM, which is in a range of 120–140 nm. The particles are joined together to form a cluster. The particles have a hexagonal geometry.

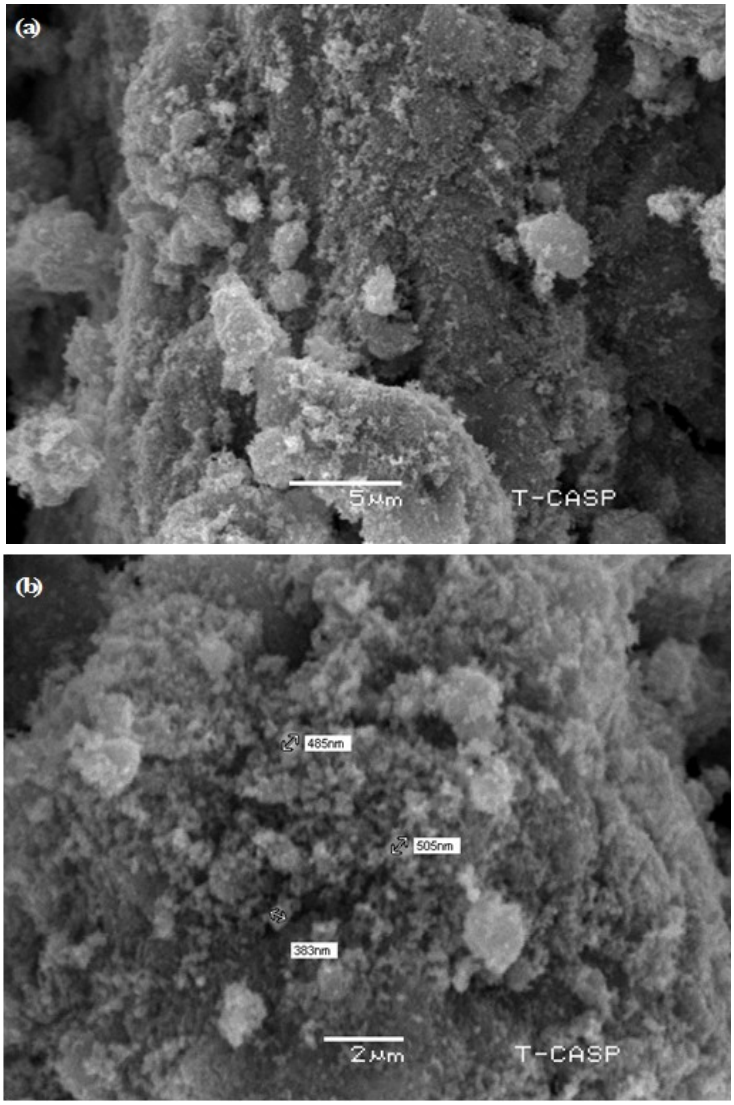


**Figure 5.** ZnO nanoparticles photoanode prepared using spin coating with magnification: (**a**) 5 µm and (**b**) 2 µm.

Figure 6 shows the nanorods on seeded and unseeded substrates. The images show the formation of nanorods on the ITO substrate. Figure 3a shows the unseeded nanorods-based photoanodes. The rods are uneven with a variable diameter and length ranging from 100 to 200 nm. The nanorods are not the same dimensions. The shape of the rods is similar to hexagonal geometry. However, the seeded substrate with Ca-doped ZnO nanorods shows highly ordered, symmetric and hexagonal-shaped vertical nanorods. The seed layer provides better nanorods sticking and growth, which results in a highly smooth and ordered nanostructural growth. The diameter of the Ca-doped ZnO nanorods deposited on the seeded substrate is in the range of 160–250 nm with a length of 0.5–1.5 µm. The rods are highly dense and symmetric.

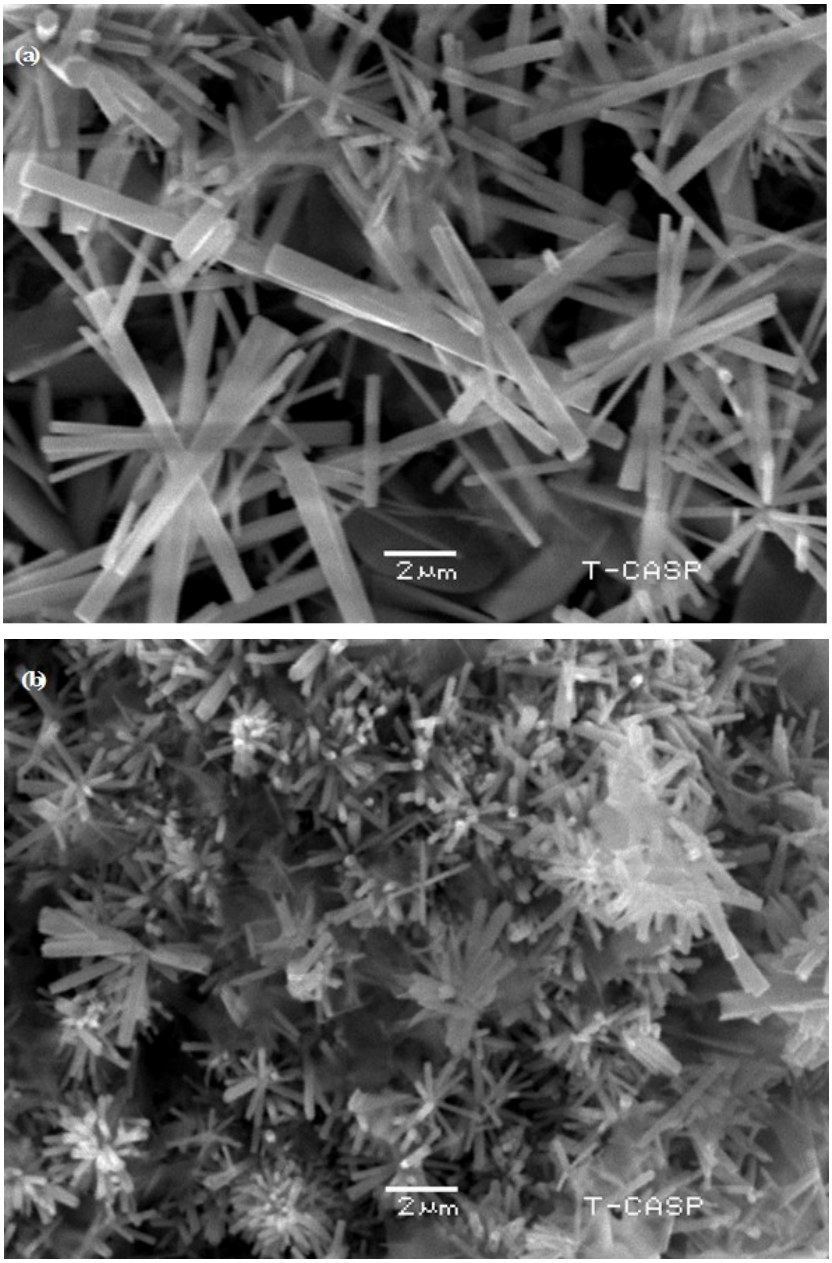


**Figure 6.** (**a**) Ca-doped ZnO nanorods on unseeded substrate; (**b**) Ca-doped ZnO nanorods on seeded substrate.

EDX analysis was also performed to study the chemical composition of the prepared photoanodes. Figure 7 shows the presence of calcium, zinc, and oxygen in the prepared seeded Ca-doped ZnO

nanorods-based photoanodes. The presence of these three chemicals shows the purity of the prepared photoanodes without the incorporation of any impurities. The EDX graphs show the proper doping of calcium in the ZnO nanostructure.

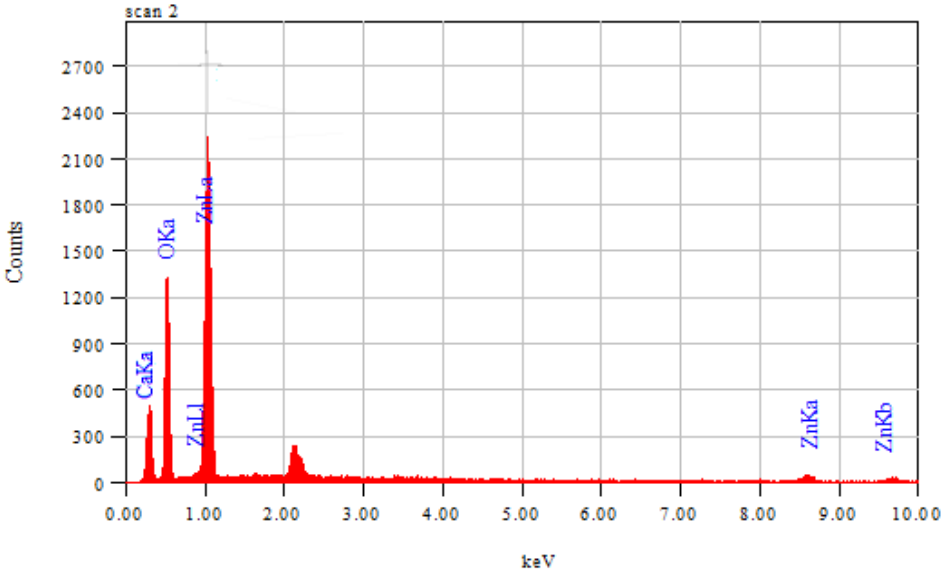


**Figure 7.** EDX spectrum of the seeded Ca-doped ZnO nanorods.

Table 3 shows the atomic percentage of the above stated elements. The table shows that the Ca elements are completely incorporated in the ZnO nanostructure. The prepared anodes are pure and contain no impurity.

**Table 3.** Atomic percentage of Zn, O, and Ca present in the prepared photoanodes.

| **Detail** | **Atomic %** | | |
|---|---|---|---|
| **Elements** | **Zinc** | **Oxygen** | **Calcium** |
| Ca-doped ZnO nanoparticles | 45.32 | 2.59 | 52.09 |
| Unseeded Ca-doped ZnO nanorods | 48.9 | 2.3 | 48.8 |
| Seeded Ca-doped ZnO nanorods | 46.55 | 1.99 | 51.46 |

The XRD graph for the Ca-doped ZnO nanoparticles photoanodes is shown in Figure 8. The graph shows the presence of zinc oxide and calcium. The low-intensity peaks at $2\theta$ = 29.51, 43.3, and 45.51 indicate the presence of calcium in the prepared Ca-doped ZnO nanoparticle photoanodes. The major peaks at $2\theta$ = 31.7, 34.5, 47.58, 54.59, and 69.88 show the peak of ZnO with a wurtizle hexagonal structure of ZnO. The high-intensity peak of ZnO shows that the photoanode is commonly composed of ZnO. However, the small intensity peaks of calcium confirm the incorporation of Ca in the ZnO nanostructure and the formation of Ca-doped ZnO nanoparticles.

Figure 9 shows the XRD graph of unseeded and seeded Ca-doped ZnO nanorods using chemical bath deposition. The peaks of ZnO and Ca are in accordance with the Ca-doped ZnO nanoparticles. The intensity of the most dominant diffraction peaks of ZnO (002), (101), and (102) shows an increase in seeded substrate. This effect is due to the formation of more aligned and symmetric nanorods. The incorporation of Ca in the ZnO wurtizle hexagonal structure can also be confirmed using the XRD graph.

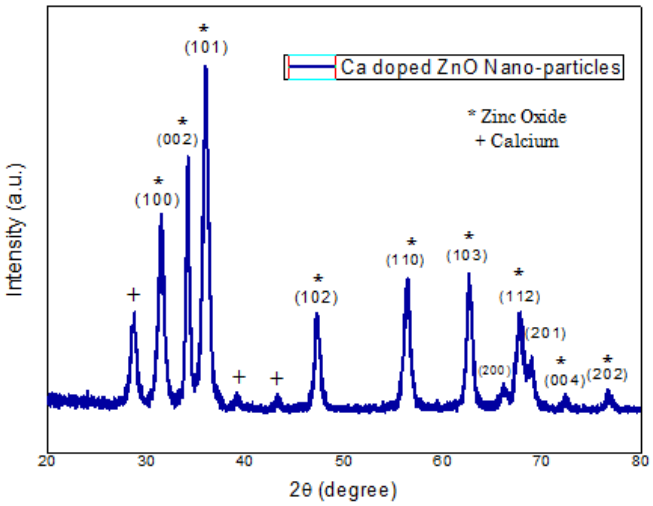


**Figure 8.** XRD spectra of Ca-doped ZnO nanoparticles.

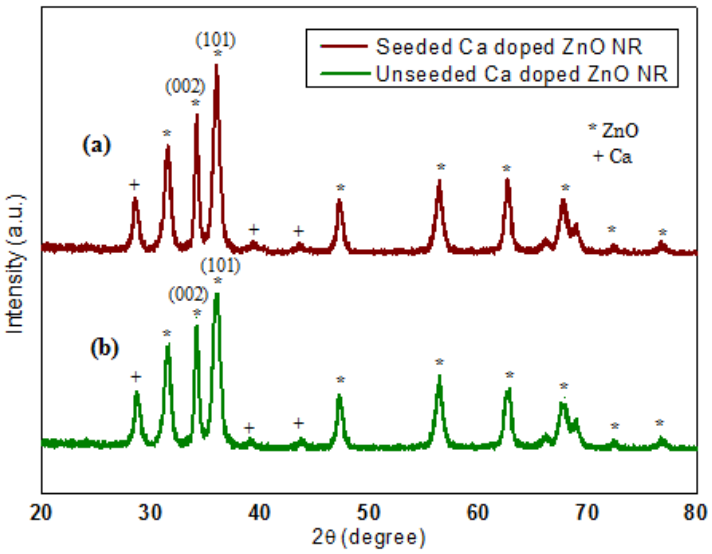


**Figure 9.** XRD graph of (**a**) Seeded Ca-doped ZnO NR and (**b**) Unseeded Ca-doped ZnO NR.

The UV-Vis spectroscopy results show the maximum absorbance based on the absorbance onset on a specific wavelength. Using this absorbance onset value, the band gap of the sample can be calculated using the Tauc plot. Figure 10 shows the UV-Vis spectroscopy results of the as-prepared Ca-doped ZnO nanoparticles, as well as the seeded and unseeded Ca-doped ZnO nanorods. The spectra consist of three portions. The first part is a slope indicating an absorption edge. The second part is a plateau region where absorption seems constant or shows a gradual change with increasing wavelength. The third part is the second absorption edge. The wavelengths of each sample are obtained by the tangential fitting of the linear portion of the spectrum, which is called the cut-off wavelength, and this gives the onset wavelength of light that is absorbed. The band gap of the prepared films are calculated using the Tauc plot by using $\alpha h\nu = A(h\nu - E_g)^n$, where A is the absorption co-efficient. Using the Tauc plot of the prepared Ca-doped ZnO NP, seeded Ca-doped ZnO NR, and unseeded Ca-doped ZnO NR, the band gap of the Ca-doped ZnO NP is equal to 3.13 eV, the unseeded Ca-doped ZnO NR is 3.15 eV, and the seeded Ca-doped ZnO NR is 3.18 eV. The increase in band gap can be attributed to the increase in the nanorods diameter. Furthermore, the increase in the band gap of the photoanode of DSSC will increase the open circuit voltage, which will result in the enhancement of the overall solar cell efficiency. Similarly, there is a decrease in the band gap of the prepared Ca-doped ZnO nanorods

from the already reported band-gap value of ZnO nanorods. This effect is mainly due to the addition of a highly conductive second group element—i.e., Ca in a ZnO lattice.

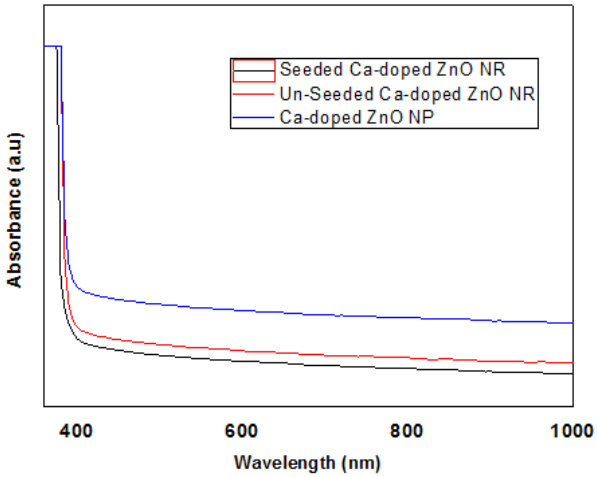


**Figure 10.** UV-Vis absorption graph of Ca-doped ZnO nanoparticles, unseeded nanorods, and seeded nanorods.

The effect of using seeded and unseeded NR as a photoanode on the overall performance of the DSSC is also studied. The open circuit voltage, short circuit current, and fill factor are estimated using a solar simulator. The overall efficiency of the cell is calculated using the above quantities and Equation (1),

$$\eta = \frac{Voc\ Isc\ FF}{Pin} \quad (1)$$

where *Pin* is the input power. Figure 11 shows the short circuit current density for the respective open circuit voltage.

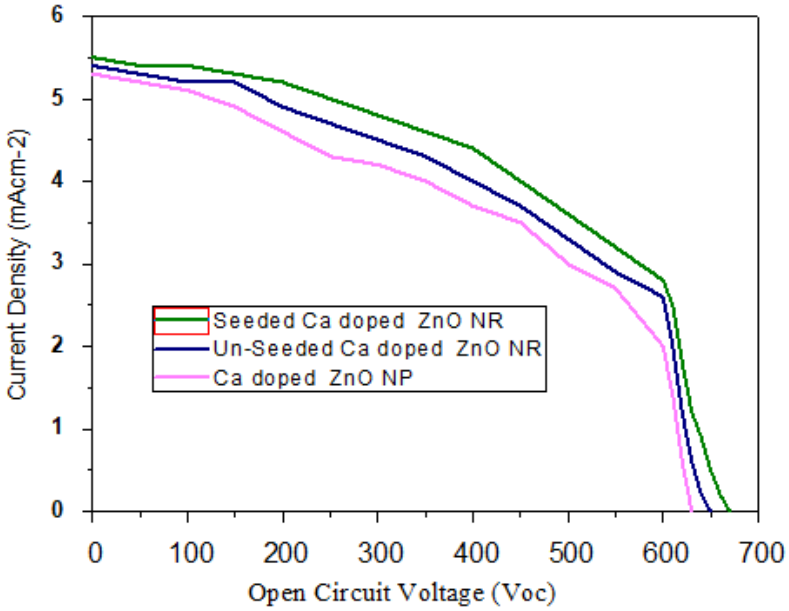


**Figure 11.** Photovoltaic characteristic plot of Ca-doped ZnO nanoparticles, unseeded nanorods, and seeded nanorods.

Table 4 shows the open circuit voltage, short circuit current, fill factor, and efficiency of the prepared Ca-doped ZnO NP and Ca-doped ZnO NR when used as a photoanode in DSSC.

**Table 4.** Comparison of photovoltaic parameters for the prepared photoanodes.

| Sample | $V_{oc}$ (V) | $J_{sc}$ (mAcm$^{-2}$) | Fill Factor | Efficiency η (%) |
|---|---|---|---|---|
| Ca-doped ZnO NP | 0.63 | 5.3 | 0.36 | 1.20 |
| Unseeded Ca-doped ZnO NR | 0.65 | 5.4 | 0.39 | 1.36 |
| Seeded Ca-doped ZnO NR | 0.67 | 5.5 | 0.42 | 1.55 |

The solar cell efficiency of the cell is the highest for seeded Ca-doped ZnO NR. The efficiency of 1.55% of seeded Ca-doped ZnO NR is mainly due to less series resistance. A thin layer of ZnO deposited before the Ca-doped ZnO NR provide enhanced charge transform due to the even growth of nanorods. The small efficiency of Ca-doped ZnO NP is mainly due to the higher grain boundaries effect in nanoparticles, which results in a small charge transfer. Small Voc can be attributed to large amount of electron–hole pair recombination.

## 5. Conclusions

In this work, a comparative study has been performed to envisage the structural and optical properties of Ca-doped ZnO NP with seeded and unseeded Ca-doped ZnO NR. Simulation has been performed in fuzzy logic controller. The simulation depicts that based on the rules, the simulated and calculated values show an error of less than 1%. The incorporation of Ca in ZnO nanocrystal is confirmed using XRD and EDX spectrum. A SEM image shows the formation of nanoparticles and nanorods in the prepared photoanodes. The band gap as well as the diameter of the seeded Ca-doped ZnO NR is greater than that of unseeded Ca-doped ZnO NR. The photovoltaic parameters of the prepared photoanodes were also studied for dye-sensitized solar cells. The results depict that the seeded Ca-doped ZnO NR shows the highest solar cell power conversion efficiency of 1.55%. The increase can be attributed to the decrease in series resistance due to the more aligned nanostructure.

**Author Contributions:** S.T., M.W.A. and V.E.B. have contributed in Conceptualization, Funding acquisition, Investigation, Methodology, Project administration, Resources, Software; S.T., M.W.A. and M.A. contributed the Writing—original draft; M.I.T., M.A., N.W. and M.M.B., contributed in Formal analysis, Supervision, Validation, Visualization, Writing—review & editing. All authors have read and agreed to the published version of the manuscript.

**Funding:** This research received no external funding.

**Acknowledgments:** Authors would like to acknowledge Managing Editor, Energies MDPI, Helen Li, for providing authors discount voucher to manage the publication fee of this manuscript. The authors are also thankful to Nano-electronics Research Lab, GC University Lahore, for providing facilities during this research.

**Conflicts of Interest:** The authors have no conflicts of interest.

## References

1. Selopal, G.S.; Zhao, H.; Tong, X.; Benetti, D.; Navarro-Pardo, F.; Zhou, Y.; Barba, D.; Vidal, F.; Wang, Z.M.; Rosei, F. Highly Stable Colloidal "Giant" Quantum Dots Sensitized Solar Cells. *Adv. Funct. Mater.* **2017**, *27*, 1701468. [CrossRef]
2. Mehmood, U.; Rahman, S.-U.; Harrabi, K.; Hussein, I.; Reddy, B.V.S. Recent Advances in Dye Sensitized Solar Cells. *Adv. Mater. Sci. Eng.* **2014**, *2014*, 1–12. [CrossRef]
3. O'Regan, B.; Grätzel, M.; Gr, M. A low-cost, high-efficiency solar cell based on dye-sensitized colloidal $TiO_2$ films. *Nature* **1991**, *353*, 737–740. [CrossRef]
4. Ince, M.; Yum, J.-H.; Kim, Y.; Mathew, S.; Grätzel, M.; Torres, T.; Nazeeruddin, M.K. Molecular Engineering of Phthalocyanine Sensitizers for Dye-Sensitized Solar Cells. *J. Phys. Chem. C* **2014**, *118*, 17166–17170. [CrossRef]
5. Ardo, S.; Meyer, G.J. Photodriven heterogeneous charge transfer with transition-metal compounds anchored to TiO2semiconductor surfaces. *Chem. Soc. Rev.* **2009**, *38*, 115–164. [CrossRef] [PubMed]

6. Suhaimi, S.; Mukhzeer, M.S.; Alahmed, Z.; Chyský, J.; Reshak, A.H. Materials for Enhanced Dye-sensitized Solar Cell Performance: Electrochemical Application. *Int. J. Electrochem. Sci.* **2015**, *10*, 2859–2871.
7. Akhlaq, M.; Khan, Z.S. Synthesis and characterization of electro-spun $TiO_2$ and $TiO_2$-$SnO_2$ composite nano-fibers for application in advance generation solar cells. *Mater. Res. Express* **2020**, *7*, 015523. [CrossRef]
8. Dembele, K.T.; Selopal, G.S.; Soldano, C.; Nechache, R.; Rimada, J.C.; Concina, I.; Sberveglieri, G.; Rosei, F.; Vomiero, A. Hybrid Carbon Nanotubes–$TiO_2$ Photoanodes for High Efficiency Dye-Sensitized Solar Cells. *J. Phys. Chem. C* **2013**, *117*, 14510–14517. [CrossRef]
9. Hossain, M.K.; Al Mortuza, A.; Sen, S.K.; Basher, M.; Ashraf, M.; Tayyaba, S.; Mia, M.; Uddin, M.J. A comparative study on the influence of pure anatase and Degussa-P25 $TiO_2$ nanomaterials on the structural and optical properties of dye sensitized solar cell (DSSC) photoanode. *Optik* **2018**, *171*, 507–516. [CrossRef]
10. Rani, R.; Sharma, S. Preparation and Characterization of $SnO_2$ Nanofibers via Electrospinning. *Adv. Nanoparticles* **2016**, *5*, 53–59. [CrossRef]
11. Martinson, A.B.F.; Elam, J.W.; Hupp, J.T.; Pellin, M. ZnO Nanotube Based Dye-Sensitized Solar Cells. *Nano Lett.* **2007**, *7*, 2183–2187. [CrossRef] [PubMed]
12. Gong, J.; Liang, J.; Krishnan, S. Review on dye-sensitized solar cells (DSSCs): Fundamental concepts and novel materials. *Renew. Sustain. Energy Rev.* **2012**, *16*, 5848–5860. [CrossRef]
13. Liu, X.; Yuan, R.; Liu, Y.; Zhu, S.; Lin, J.; Chen, X. Niobium pentoxide nanotube powder for efficient dye-sensitized solar cells. *New J. Chem.* **2016**, *40*, 6276–6280. [CrossRef]
14. Kim, K.H.; Utashiro, K.; Abe, Y.; Kawamura, M. Structural Properties of Zinc Oxide Nanorods Grown on Al-Doped Zinc Oxide Seed Layer and Their Applications in Dye-Sensitized Solar Cells. *Materials* **2014**, *7*, 2522–2533. [CrossRef]
15. Ali, B.; Ashraf, M.W.; Tayyaba, S. Simulation, Fuzzy Analysis and Development of ZnO Nanostructure-based Piezoelectric MEMS Energy Harvester. *Energies* **2019**, *12*, 807. [CrossRef]
16. Basher, M.K.; Khalid Hossain, M.; Afaz, R.; Tayyaba, S.; Akand, M.A.R.; Rahman, M.T.; Eman, N.M. Study and investigation of phosphorus doping time on emitter region for contact resistance optimization of monocrystalline silicon solar cell. *Results Phys.* **2018**, *10*, 205–211. [CrossRef]
17. Yangyang, Z.; Manoj, K.R.; Elias, K.S.; Yogi, D.G. Synthesis, Characterization, and Applications of ZnO Nanowires. *J. Nanomater.* **2012**, *2012*, 22.
18. Umar, A.; Singh, P.; Al-Ghamdi, A.A.; Al-Heniti, S. Direct growth of ZnO nanosheets on FTO substrate for dye-sensitized solar cells applications. *J. Nanosci. Nanotechnol.* **2010**, *10*, 6666–6671. [CrossRef]
19. Wahyuono, R.A.; Schmidt, C.; Dellith, A.; Dellith, J.; Schulz, M.; Seyring, M.; Rettenmayr, M.; Plentz, J.; Dietzek, B. ZnO nanoflowers-based photoanodes: Aqueous chemical synthesis, microstructure and optical properties. *Open Chem.* **2016**, *14*, 158–169. [CrossRef]
20. Sunandan, B.; Joydeep, D. Hydrothermal growth of ZnO nanostructures. *Sci. Technol. Adv. Mater.* **2009**, *10*, 13001.
21. Gupta, A.K.; Kashyap, V.; Gupta, B.K.; Nandi, S.P.; Saxena, K.; Khare, N. Synthesis of ZnO Nanorods by Electrochemical Deposition Method and Its Antibacterial Activity. *J. Nanoeng. Nanomanufact.* **2013**, *3*, 348–352. [CrossRef]
22. Wu, J.-J.; Liu, S.-C. Low-Temperature Growth of Well-Aligned ZnO Nanorods by Chemical Vapor Deposition. *Adv. Mater.* **2002**, *14*, 215–218. [CrossRef]
23. Seung, C.L.; Ye, Z.; Cheol, J.L.; Hyun, R.; Hwack, J.L. Low-Temperature Growth of ZnO Nanowire Array by a Simple Physical Vapor-Deposition Method. *Chem. Mater.* **2003**, *15*, 3294–3299.
24. Mahshid, P.; Pirooz, M.; Davoud, H.F.; Mohammadreza, K.E. Synthesis of ZnO nanorods via chemical bath deposition method: The effects of physicochemical factors. *Ceram. Int.* **2016**, *42*, 173–184.
25. Polat, I.; Yılmaz, S.; Tomakin, M.; Bacaksız, E. Role of Mg doping in the structural, optical, and electrical characteristics of ZnO-based DSSCs. *Turk. J. Phys.* **2017**, *41*, 160–170. [CrossRef]
26. Istrate, A.-I.; Nastase, F.; Mihalache, I.; Comanescu, F.; Gavrila, R.; Tutunaru, O.; Romanitan, C.; Tucureanu, V.; Nedelcu, M.; Müller, R. Synthesis and characterization of Ca doped ZnO thin films by sol–gel method. *J. Sol-Gel Sci. Technol.* **2019**, *92*, 585–597. [CrossRef]
27. Mahdhi, H.; Djessas, K.; Ben Ayadi, Z. Synthesis and characteristics of Ca-doped ZnO thin films by rf magnetron sputtering at low temperature. *Mater. Lett.* **2018**, *214*, 10–14. [CrossRef]
28. Gul, M.; Amin, D.; Abbas, M.; Ilyas, S.; Shah, N. Synthesis and characterization of magnesium doped ZnO nanostructures: Methane ($CH_4$) detection. *J. Mater. Sci. Mater. Electron.* **2019**, *30*, 5257–5265. [CrossRef]

29. Sarwar, G.; Ashraf, M.W. Parametric estimation of Group II element doped zinc oxide nanostructures using fuzzy logic. *J. Intell. Fuzzy Syst.* **2020**, *38*, 5865–5875. [CrossRef]
30. Das, N.; Wongsodihardjo, H.; Islam, S. Modeling of multi-junction photovoltaic cell using MATLAB/Simulink to improve the conversion efficiency. *Renew. Energy* **2015**, *74*, 917–924. [CrossRef]
31. Wasim, M.F.; Tayyaba, S.; Ashraf, M.W.; Ahmad, Z. Modeling and Piezoelectric Analysis of Nano Energy Harvesters. *Sensors* **2020**, *20*, 3931. [CrossRef] [PubMed]
32. Wasim, M.F.; Ashraf, M.W.; Tayyaba, S.; Nazir, A.S. Simulation and synthesis of ZnO nanorods on AAO nano porous template for use in a MEMS devices. *Dig. J. Nanomater. Biostruct.* **2019**, *14*, 559–567.